A Two Transition State Model for Radical−Molecule Reactions: Applications to Isomeric Branching in the OH−Isoprene Reaction

Erin E. Greenwald,[†] Simon W. North,*[,†] Yuri Georgievskii,[‡] and Stephen J. Klippenstein*[,§]

Department of Chemistry, Texas A&M University, P.O. Box 30012, College Station, Texas 77842, Combustion Research Facility, Sandia National Laboratories, Livermore, California 94551-0969, and Chemistry Division, Argonne National Laboratories, Argonne, Illinois 60439-4831

Received: February 19, 2007; In Final Form: April 18, 2007

A two transition state model is applied to the prediction of the isomeric branching in the addition of hydroxyl radical to isoprene. The outer transition state is treated with phase space theory fitted to long-range transition state theory calculations on an electrostatic potential energy surface. High-level quantum chemical estimates are applied to the treatment of the inner transition state. A one-dimensional master equation based on an analytic reduction from two-dimensions for a particular statistical assumption about the rotational part of the energy transfer kernel is employed in the calculation of the pressure dependence of the addition process. We find that an accurate treatment of the two separate transition state regions, at the energy and angular momentum resolved level, is essential to the prediction of the temperature dependence of the addition rate. The transition from a dominant outer transition state to a dominant inner transition state is shown to occur at about 275 K, with significant effects from both transition states over the 30−500 K temperature range. Modest adjustments in the ab initio predicted inner saddle point energies yield predictions that are in quantitative agreement with the available high-pressure limit experimental observations and qualitative agreement with those in the falloff regime. The theoretically predicted capture rate is reproduced to within 10% by the expression $[1.71 \times 10^{-10}(T/298)^{-2.58} \exp(-608.6/RT) + 5.47 \times 10^{-11}(T/298)^{-1.78} \exp(-97.3/RT)$; with $R = 1.987$ and T in K] cm^3 molecule^{-1} s^{-1} over the 30−500 K range. A 300 K branching ratio of 0.67:0.02:0.02:0.29 was determined for formation of the four possible OH−isoprene adduct isomers **1**, **2**, **3**, and **4**, respectively, and was found to be relatively insensitive to temperature. An Arrhenius activation energy of −0.77 kcal/mol was determined for the high-pressure addition rate constants around 300 K.

I. Introduction

The photochemical oxidation of biogenic non-methane organic compounds (NMOCs) contributes greatly to tropospheric ozone production.[1−3] Isoprene (2-methyl-1,3-butadiene) is the largest single source biogenic NMOC emitted worldwide with an emission rate in excess of ∼500 Tg C yr^{-1}.[3] Hydroxyl radical initiated photooxidation of isoprene directs much of the ground level ozone production in North America during summer months. Isoprene oxidation is also thought to contribute to secondary organic aerosol (SOA) formation via further reactions of first-generation end products in both high- and low-NO_x conditions[4−8] and to contribute to hygroscopic SOA formation through cloud processing.[9−12] The detailed mechanism of the OH initiated oxidation of isoprene has been the focus of numerous recent studies.

Electrophilic addition of OH to isoprene is the dominant mechanism under tropospheric conditions. Isotopomeric kinetics experiments performed by Campuzano-Jost et al.[18] determined that there are no H/D kinetic isotope effects in the temperature regime relevant to the troposphere (250−340 K), for the reaction of OH with isoprene, which confirms the addition mechanism. The OH addition to isoprene results in four distinct hydroxyalkyl radicals (**1**−**4**), with an overall second-order reaction rate constant of

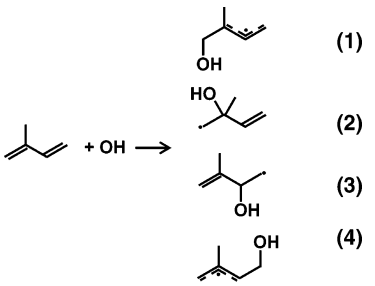

approximately 1×10^{-10} cm^3 molecule^{-1} s^{-1} at 298 K.[1,13−31] Temperature-dependent studies reveal a modest inverse temperature dependence for temperatures of tropospheric relevance.[1,17,18,21,23,27,31]

The atmospheric importance of this reaction has generated abundant experimental data as a function of both temperature and pressure. The advent of Pulsed Laval Nozzle measurements, including those of Spangenberg and co-workers,[28] allow an extension of ambient measurements to very low temperatures. The majority of the experiments performed focus on the high-pressure limit[14−16,18−23,25,27,28,30] with a few experiments performed in the 1−10 Torr range to examine falloff behavior.[24,25,29,31] The branching ratios of isoprene−OH adducts (where the numerals **1**−**4** indicate the carbon site of attack in

[†] Texas A&M University.
[‡] Sandia National Laboratories.
[§] Argonne National Laboratories.

10.1021/jp071412y CCC: $37.00
Published on Web 06/01/2007

accordance with the above schematic) influences the distribution of first-generation end products. The generally accepted mechanism describing the subsequent reactivity of these hydroxyalkyl radicals in the presence of O_2 involves O_2 addition to all four OH−isoprene adducts to form the corresponding peroxy radicals.[1,2,20,32,38,59] Recently, computational studies by Park et al. demonstrated that OH−isoprene adducts **2** and **3** react primarily via a prompt cyclic isomerization to produce α-hydroxyalkyl radicals, which subsequently undergo hydrogen abstraction by O_2.[33]

To explore this new chemistry, Greenwald et al. performed an isomeric-selective study for the case of OH addition to the inner position of butadiene.[34] Isomeric selectivity was achieved by the preparation of a photolytic precursor, which, upon photolysis, formed the primary radical resulting from the OH addition to butadiene. The study supported the cyclic isomerization pathway and the computational predictions of Park et al. Subsequent work by Greenwald et al. to produce the isoprene−OH hydroxyalkyl radicals provides a more direct confirmation of this pathway in the case of isoprene oxidation.[35] The addition of OH to one of the inner positions of isoprene will lead to primarily C5-carbonyl products and HO_2, both of which have been observed in the end product analysis of Lee et al.[38] and Paulson et al.[62] Therefore, verification of this pathway provides additional insight into the origins of observed products. Furthermore, these isomeric experiments provide a stringent test for theory.

Experimental determination of the branching ratio, however, has proven to be challenging. Almost all the analysis and interpretation of accurate experimental results is based on a branching ratio determined using structure additivity relationships (SAR) developed by Peeters et al.,[36] slightly adjusted to provide a fit to the data. SARs have been used to determine relative branching for the addition of hydroxyl radicals to a number of alkenes.[36,37] Several experimental studies have attempted to ascertain the branching ratio using OH cycling[26] or end-product distributions.[29,38]

Theoretical studies of the kinetics have also been performed.[24,29,39,40] Here, we will present a new theoretical model and compare its predictions with a large set of experimental observations. This model improves on the prior models in a variety of ways. First, our model is based on a higher level and more complete quantum chemical analysis. Furthermore, this quantum chemical analysis is carefully benchmarked against higher level calculations for the much smaller ethylene + OH system. Perhaps more importantly, we make significant improvements in the transition state theory parts of the kinetic analysis. In particular, a key aspect of the addition of OH radicals to alkenes involves the presence of two distinct transition state regions. An outer transition state describes the initial formation of a long-range van der Waals complex, whereas an inner transition state describes the transformation from the van der Waals complex to a chemical adduct. Here, the combined effect of these two transition states is treated at an energy, *E*, and total angular momentum, *J*, resolved level. Other models have either simply neglected the outer transition state or else employed wholly inadequate treatments of its effect. Finally, we also include a master equation analysis based on an analytic reduction of the two-dimensional master equation to one-dimensional for a particular statistical assumption about the rotational part of the energy transfer kernel.

The two-transition state Rice−Ramsperger−Kassel−Marcus (RRKM) theory coupled with a master equation (ME) treatment employed here was previously used to model the addition of hydroxyl radicals to ethylene and provided excellent agreement with the extensive available temperature- and pressure-dependent experimental data.[41] The ethylene−OH system permits benchmarking of various aspects of the present treatment such as the level of theory used in the quantum chemical calculations, inclusion of variational effects, the effects of tunneling, hindered rotor treatments of low-frequency motions, and anharmonicity, as well as the significance of including both an outer and an inner transition state. In the ethylene−OH system, at 300 K, the *E*,*J*-resolved effective rate was 30% lower than that predicted by inclusion of only the inner transition state. This divergence should increase as the inner saddle point lowers in energy. Including only the inner transition state was found to be an inadequate representation of the kinetics below temperatures comparable to the energy of the saddle point below the reaction asymptote. In the isoprene−OH system, the energies of the saddle points for formation of the four isomers are 2.43, 0.94, 0.08, and 2.13 kcal/mol (including zero point energy) below the reaction asymptote for isomers **1**−**4**, respectively. This implies that inclusion of only the inner transition state will be insufficient below temperatures as high as about 1200 K.

The models we employ for the inner and the outer transition states are distinctly different. The outer transition state lies at large separations, beyond the van der Waals minimum, where only long-range interactions are important. Considerable effort has been devoted to the implementation of quantized versions of transition state theory for such long-range potentials to obtain accurate estimates for the low-temperature limit rate. Here, we are more interested in somewhat higher temperatures (e.g., above about 10 K), with our primary focus on understanding where the transition from the long-range to the short-range transition state occurs. In this temperature range a recently derived classical long-range transition state theory approach is appropriate.[42] The derivation of this approach included an application to the addition of hydroxyl radical to isoprene, and the results of this analysis provide the basis for the present treatment of the outer transition state.

The inner transition state region for the isoprene + OH reaction is somewhat more complex than for ethylene + OH as there are now four separate inner transition states corresponding to the formation of the four different isomers of the adduct. Each inner transition state is near a saddle point on the potential energy surface. The saddle point arises as the chemical bond between the carbon and oxygen atoms forms and the CC Π bond weakens. The interplay between these two chemical forces determines the precise location of the saddle point, which corresponds to carbon-oxygen separations of 2.1−2.35 Å for the four different isomers (**1**−**4**). At such short separations, the intermolecular forces between the isoprene and hydroxyl moieties are quite strong. As a result, a simple rigid-rotor harmonic-oscillator treatment of all but the HOCC torsional modes, the cis−trans isomer conversion modes, and the torsional modes of the methyl rotations, which are treated as one-dimensional (1D) hindered rotors, provides a reasonably satisfactory treatment of the inner transition state. A standard energy, *E*, and total angular momentum, *J*, resolved RRKM kinetics analysis is then performed to evaluate the reaction rates.

The computational methodologies employed for both the ab initio determinations, and for the kinetics evaluations are summarized in section II. In section III, the quantum chemical results and the predictions for the rate constants are presented and discussed. This discussion focuses on a comparison with experiment and on the effect of the transition from a dominant outer to a dominant inner transition state as the temperature

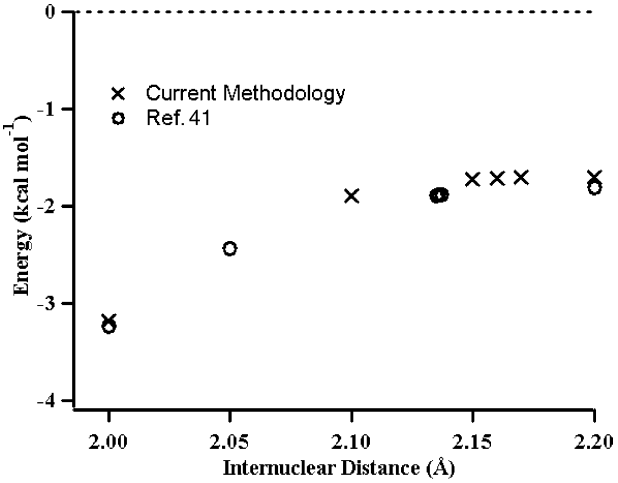

Figure 1. Energies in the region of the inner saddle point for the C_2H_4 + OH reaction employing the current computational scheme (eq 1, Xs) as compared to the previously published extrapolation scheme of ref 41 (circles). Energies are relative to an infinite separation energy of the C_2H_4 + OH of 0 kcal/mol in both cases. Zero point energy is not included.

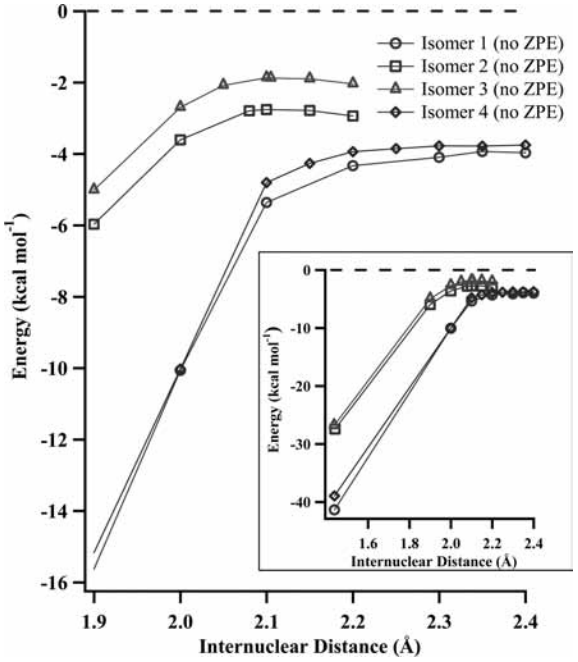

Figure 2. Reaction coordinate diagrams, in the region of the inner transition state, with relative energy (eq 1) as a function of C−O separation for the formation of each of the four isomers. Zero point energy is not included. (There is also no correction for the spin−orbit splitting of OH.)

rises as well as providing an accurate prediction of the initial branching ratio under tropospheric conditions. Some concluding remarks are provided in section IV.

II. Computational Methodology

A. Ab Initio Calculations. The focus of the present ab initio quantum chemical calculations is the accurate evaluation of the rovibrational properties of the reactants, the products, and of the reaction path in the transition state region. All geometry optimizations used for the kinetics simulations were performed using the unrestricted Becke-3 Lee−Yang−Parr (uB3LYP)[43] density functional with the Pople-style triple-ζ polarized split-valence basis sets with diffuse functions 6-311++G**[44,45] as implemented in the Gaussian 03 suite of programs.[46] Single point energy calculations were performed on those geometries using restricted open-shell quadratic configuration interaction calculations with perturbative inclusion of the triples contribution (roQCISD(T)),[47] employing the Pople-style double-ζ polarized split valence basis sets with diffuse functions, 6-31++G**, as well as using restricted open-shell Möller−Plesset perturbation theory (roMP2)[48] employing both the 6-31++G** basis sets and the Pople-style triple-ζ polarized split valence basis sets with diffuse functions 6-311++G(3df,2pd) as employed in the Molpro suite of programs.[49]

When the equilibrium structures of the individual isoprene−OH adducts are considered, care must be taken to ensure that the global minimum for each structure is determined. In the deep wells of the adducts, many local minima corresponding to different rotational isomers of the adducts exist. As such, B3LYP/6-31G*[50] was used to optimize structures and calculate energies to determine the lowest energy rotational conformation of each isoprene−OH adduct. For the four isoprene−OH adducts, 58 local minima were found. The optimized geometry of the lowest energy conformation for each adduct was then used as the starting geometry for all subsequent calculations.

We have re-examined the ethylene−OH potential energy surface (PES) in the region of the inner transition state to develop a more tractable methodology, i.e., one which is computationally less expensive than was used in the ethylene−OH study but that quantitatively captures the high-level potential energy surface. Figure 1 is a plot of energy vs C−O internuclear separation for the ethylene−OH system calculated at the roQCISD(T)/6-31++G**//B3LYP/6-311++G** level of theory including a basis set correction at the roMP2 level of theory (X's in Figure 1) as described by

$$E_\infty = [\text{roQCISD(T)/6-31++G**//B3LYP/6-311++G**}] + [\text{roMP2/6-311++G(3df,2pd)//B3LYP/6-311++G**}] - [\text{roMP2/6-31++G**//B3LYP/6-311++G**}] \quad (1)$$

Overlaid in Figure 1 (circles) is the plot of energy vs C−O internuclear separation for calculations at the more computationally expensive method published previously.[41] The saddle point optimized along the C−O internuclear-separation employing the present methodology is within 0.015 Å and 0.17 kcal mol^{-1} of that previously reported.

Given the success of the above computational methodology, we have adopted this approach to treat the isoprene−OH system as shown in Figure 2. In the case of isomers **2** and **3**, direct B3LYP/6-311++G** saddle point optimizations located a transition state along the reaction coordinate and these were used in subsequent calculations. However, no such transition states were found for isomers **1** and **4**. Instead, constrained geometry optimizations at the B3LYP/6-311++G** level of theory, along a coordinate of C−O internuclear separation, were performed. Saddle points at the composite level of eq 1 were then found along the individual PESs. The energies from those calculations were used to construct the present PESs.

Harmonic frequencies and rigid rotor rotational constants were calculated for all stationary points at the B3LYP/6-311++G** level and those frequencies were used to include zero point energy. Vibrational frequencies obtained for the stationary points are given in Table 1. One-dimensional torsional potentials were calculated. Isomers **1** and **4** have three hindered rotors each, which correspond to the methyl rotations, the CC−OH torsional motions, and the OC−CC isomerization motions. Isomers **2** and **3** have four hindered rotors each, which correspond to the methyl

TABLE 1: Frequencies of Stationary Points

species	frequencies (B3LYP/6-311++G**)													
isoprene	162	201	278	410	431	536	644	783	790	927	936	960	1011	1027
	1068	1088	1324	1328	1410	1429	1458	1483	1502	1652	1692	3023	3070	3109
	3131	3135	3144	3217	3223									
Exp.[55]	153	199	288	401	412	523	622	755	780	891	903	953	990	1012
	1034	1069	1219	1303	1388	1414	1425	1442	1466	1603	1638	2910	2928	2956
	2978	2988	3020	3092	3097									
OH	3709													
exp[64]	3738													
TS 1	138i	74	85	144	175	180	281	410	426	537	566	661	782	795
	935	944	961	1011	1019	1056	1086	1322	1338	1406	1421	1454	1479	1500
	1596	1646	3027	3076	3126	3134	3147	3159	3230	3254	3762			
TS 1[a]	72	85	142	175	178	281	406	426	537	563	661	780	795	923
	944	961	1011	1018	1055	1086	1322	1338	1406	1421	1454	1479	1500	1596
	1645	3027	3076	3126	3134	3147	3152	3230	3249	3755				
TS 2	269i	118	187	201	227	267	297	364	419	528	599	712	730	779
	867	955	956	1008	1023	1049	1083	1326	1331	1394	1417	1454	1479	1499
	1556	1683	3035	3106	3131	3134	3145	3148	3229	3244	3771			
TS 3	255i	76	147	176	202	265	287	424	455	532	608	704	740	793
	874	935	959	1001	1014	1070	1091	1293	1326	1408	1421	1457	1484	1504
	1568	1688	3025	3080	3114	3136	3153	3166	3219	3248	3765			
TS 4	160i	70	90	133	211	226	284	427	458	538	593	652	769	798
	926	948	963	985	1014	1069	1088	1307	1331	1408	1424	1457	1484	1507
	1593	1637	3027	3081	3114	3133	3138	3172	3222	3261	3761			
TS 4[a]	70	89	131	210	223	284	427	458	538	591	652	768	798	922
	927	961	984	1014	1069	1088	1307	1331	1408	1424	1457	1484	1507	1593
	1637	3027	3081	3114	3133	3138	3172	3222	3260	3760				
adduct 1	65	87	183	277	287	325	377	454	549	609	780	801	930	971
	985	1002	1027	1056	1179	1229	1248	1335	1384	1398	1414	1455	1493	1494
	1499	1524	2993	3005	3048	3068	3107	3116	3149	3238	3815			
adduct 2	105	115	245	280	298	323	347	418	433	547	582	699	736	878
	952	960	983	1020	1034	1044	1186	1242	1314	1320	1391	1436	1446	1482
	1490	1696	3034	3110	3114	3126	3136	3142	3223	3248	3803			
adduct 3	75	104	168	229	261	337	359	438	478	565	588	743	796	884
	933	964	1023	1058	1069	1097	1233	1282	1311	1376	1406	1443	1446	1476
	1497	1695	2944	3026	3077	3109	3124	3151	3204	3267	3825			
adduct 4	55	135	139	243	331	375	465	493	515	563	746	801	833	921
	996	1005	1032	1054	1141	1187	1272	1339	1378	1397	1420	1463	1487	1499
	1503	1516	3013	3030	3044	3081	3109	3137	3144	3232	3818			

[a] Projected frequencies.

rotations, the CC−OH torsional motions, the cis/trans isomerization motions, and the rotation of the CH_2 radical sites. Transition states **1**−**4** have two hindered rotors each, which correspond to the methyl rotations and the CC−OH torsional motions. Constrained optimizations, starting with the B3LYP/6-311++G** geometry for the lowest energy conformation of a particular stationary point, were performed as a function of dihedral angle and then the computational scheme described in eq 1 was applied. These torsional potentials were then fit to an analytical Fourier expansion (including only the first six terms) for the inclusion in density and number of state calculations.

B. Rate Calculations. To compare our theoretical results to the experimental data, which measure the overall production rates of all four isomers, one must calculate the overall rate of OH addition to isoprene. This overall production rate incorporates an effective number of states, which includes reactive flux through a long-range outer transition state in combination with the reactive flux through the shorter range inner transition state. All rate calculations, including both the high-pressure limit rate constants and those employing the master equation (ME) analysis, were carried out using the VARIFLEX code.[51]

High-Pressure Limit Rate Constants. In the case of OH addition to ethylene, a modest reduction in the ab initio predicted saddle point energy yielded a predicted capture rate which reproduced experimental data to within 10% in the temperature range from 10 to 600 K. In the present case of OH addition to isoprene, we find that a similar reduction in the ab initio predicted saddle point energy is necessary to reproduce temperature-dependent experimental observations to a similar accuracy. Variational effects were found to be small in the case of OH addition to ethylene, resulting in a reduction of the inner transition state rate constant of at most 15%, with the maximal reduction occurring at the highest temperature considered, 600 K. Additionally, in the OH addition to ethylene, the inclusion of tunneling through an Eckart barrier resulted in a non-negligible increase in the predicted inner transition state rate constant; however, this effect was pronounced only at lower temperatures, where the effect was ameliorated by the increasing dominance of the outer transition state.[41] As such, variational effects and tunneling have been neglected in the present model.

The hindered rotor replacement of the low-frequency CCOH torsional mode had the most substantial effect on the rate constant predictions in the case of OH addition to ethylene. In the present rate calculations, the low-frequency CCOH, CH_3, and cis−trans conversion torsional modes are treated with hindered rotors where applicable. For C_2H_4 + OH estimates of the effects of anharmonicities on the inner transition state were performed using phase space integral calculations, but the effects of global anharmonicities and transitional mode coupling were found to be very small. A ratio of the rate constants calculated via a phase space integral (PSI) based multifaceted-dividing-surface variable-reaction-coordinate method and calculated via the corresponding rigid-rotor harmonic oscillator method (including a hindered rotor treatment) was equal to 1.0 ± 0.1 throughout the entire temperature range from 300 to 2000 K.[41]

TABLE 2: Long-Range Transition State Theory Predictions for Rate Constants (10^{-10} cm^3 molecule^{-1} s^{-1}) for the Various Long-Range Interactions between Isoprene and OH from Ref 42

interaction potential	rate
dipole−dipole	$1.27/T^{(1/6)}$
dipole−quadrupole	3.85 (T-independent)
dipole−induced dipole	$1.27T^{(1/6)}$
dispersion forces	$2.15T^{(1/6)}$
sum	5.54[a]

[a] VTST capture rate for a potential represented by the sum of the dipole−dipole, dipole−quadrupole, dipole−induced-dipole, quadrupole−quadrupole, and the dispersion terms at 58 K.

Similarly small effects are expected here and so such global anharmonicity calculations were not repeated for the present system.

The model presented for the addition of OH to ethylene illustrated the importance of incorporating the effects from both the inner and outer transition states, in particular at the energy, E, and total angular momentum, J, resolved level. The E,J-resolved effective high-pressure addition rate constant is significantly below (i.e., by more than 10%) each of the individual rate constants all the way from 10 to 400 K. In fact, at the crossing point of the inner and outer transition state predictions, the E,J-resolved effective rate constant is more than a factor of 10 lower.[41] The present model also demonstrates the importance of including both transition states and combining the flux through each at the energy, E, and total angular momentum, J, resolved level as described in section III.

The flux through the outer transition state for the addition of OH to isoprene was explored in a recent derivation of classical variational transition state theory on long-range potentials,[42] and only a brief description of the results of that work will be presented in section III. The rate through the outer transition state is simply the long-range capture rate given by[42]

$$k_{\text{outer}} = AT^n \times 10^{-10}\ \text{cm}^3\ \text{molecule}^{-1}\ \text{s}^{-1} \qquad (2)$$

where A and n in k_{outer} are dictated by the particular long-range interaction of the potential as seen in Table 2.

To obtain the number of states, $N^{\dagger}_{\text{outer}}$, associated with the outer transition state, the number of states was calculated using classical phase space theory. The coefficient for an r^{-6} interaction potential between neutral fragments was adjusted until the phase space theory rate constant at 58 K was in agreement with the theoretical result of ref 42 when considering the sum of the electrostatic interactions.

The long-range part of the potential is fragment orientation-dependent, though the separations described by this region of the PES are sufficiently large that orientation preferences here are expected to have no bearing on reactive probability at the inner parts of the PES. As such, all four reaction channels are assumed to share a single long-range capture rate.

At large separations, there are effectively two degenerate electronic states corresponding asymptotically to the $^2\Pi_{1/2}$ and $^2\Pi_{3/2}$ states of OH. The effects of this degeneracy on the reaction coordinate near the inner transition state were considered in the ethylene−OH system and it was found that there is sufficient energetic separation (∼15 kcal/mol) of electronic states in that region of the PES that only the lowest electronic state need be considered.[41] The higher energy electronic state originating from the spin−orbit splitting of the reactant hydroxyl moiety has been neglected in this study in the region of the inner transition state. The effect of the spin−orbit coupling does, however, increase the energy at the transition state relative to reactants by 70 cm^{-1}. This shift is incorporated here.

As the inner saddle points among the four isomers vary in location and height, the reaction flux at the inner transition state for each isomer is distinct. The rate constants associated with the inner transition states for formation of each isomer are the E,J-resolved microcanonical rate constants. However, in considering the effective rate constant on the global potential energy surface, one must consider reactive flux through the inner transition state region as a whole. As such, the total reactive flux through this region of the potential energy surface related to $N^{\dagger}_{\text{inner}}$ can be considered as a series of parallel reactions where formation of each isomer is unique. The flux through the transition states can then be summed to obtain the total flux through the inner transition state region,

$$N^{\dagger}_{\text{inner}} = \sum_{i=1}^{4} N^{\dagger}_i \qquad (3)$$

where $N^{\dagger}_i$ is the reactive flux through the inner transition state corresponding to isomer i.

The inner and outer transition states act as a series of bottlenecks to reaction. A reasonable approximation to the effective flux through both transition states is given by

$$\frac{1}{N^{\dagger}_{\text{eff}}} = \frac{1}{N^{\dagger}_{\text{inner}}} + \frac{1}{N^{\dagger}_{\text{outer}}} \qquad (4)$$

where $N^{\dagger}_{\text{inner}}$ and $N^{\dagger}_{\text{outer}}$ are the E,J-resolved transition state numbers of states at the inner and outer transition states, respectively. In writing eq 4, we assume statistical probabilities for crossing each transition state dividing surface, and further that the maximum in the flux at the van der Waals minimum greatly exceeds that at the two transition states.[52,53] Given eq 3, eq 4 becomes

$$N^{\dagger}_{\text{eff}} = \frac{N^{\dagger}_{\text{outer}}[\sum_{i=1}^{4} N^{\dagger}_i]}{N^{\dagger}_{\text{outer}} + N^{\dagger}_{\text{inner}}} \qquad (5)$$

At low temperatures, the temperature dependence of the outer transition state will dominate the overall temperature dependence of the reaction rate, just as at high temperatures, the temperature dependence of the inner transition state will dictate the temperature dependence of the effective rate. At intermediate temperatures, the flux through both transition states contributes significantly to the overall rate and thusly the temperature dependence. The total reactive flux in eq 5 can be divided into the reactive probability of forming each individual isomer, providing a branching ratio $N^{\dagger}_1{:}N^{\dagger}_2{:}N^{\dagger}_3{:}N^{\dagger}_4$.

Pressure-Dependent Rate Constants. To model the pressure dependence of the system, we have employed a master equation analysis of the temperature and pressure-dependent kinetics based on an analytic reduction from two dimensions (E,J) to one dimension (E). This master equation analysis is based on the methodology described in ref 54 and assumes a particular statistical distribution for the rotational part of the energy transfer kernel. This treatment includes a temperature-dependent exponential down model of energy transfer along with Lennard-Jones collision rates. The Lennard-Jones parameters for C_5H_8OH, Ar, and He were taken to be σ = 6.02, 3.47, and 2.55 Å and ϵ = 490.2, 114.0, and 9.99 K, respectively.

TABLE 3: Relative Energies (Not Including Zero Point Energy) of the OH + Isoprene Reaction in kcal/mol

level of theory[a]	isomer **1**	isomer **2**	isomer **3**	isomer **4**
B3LYP/6-311++G** [b]	−39.8	−21.9	−22.6	−37.3
roQCISD(T)/6-31++G**//a[b]	−38.0	−25.3	−24.2	−35.5
roMP2/6-311++G(3df,2pd)//a[b]	−47.1	−32.1	−31.7	−44.0
roMP2/6-31++G**//a[b]	−43.8	−30.0	−29.1	−40.6
computational Scheme 1[b]	−41.4	−27.4	−26.8	−38.9
HF/6-31G** [c]	−31.5	−13.4	−14.6	−29.6
MP2/6-31G** [c]	−37.6	−30.2	−29.2	−34.7
MP2/6-311G** [c]	−37.3	−30.5	−29.4	−34.3
MP4(SDTQ)/6-311G**//b[c]	−35.9	−27.7	−26.4	−33.1
PMP4(SDTQ)/6-311G**//b[c]	−41.7	−28.0	−26.7	−39.1
B3LYP/6-31G** [c]	−47.7	−29.7	−30.2	−45.0

[a] "a" refers to geometry optimizations at the B3LYP/6-311++G** level of theory and "b" refers to geometry optimizations at the MP2/6-311G** level of theory [b] From current work. [c] From ref 29.

III. Results and Discussion

A. Potential Energy Surface. Results for the binding energetics of the isoprene−OH adducts, employing a variety of ab initio and density functional calculations, are tabulated in Table 3. The variation in the results confirms the need for benchmarking. Although the binding energies will only have a direct effect on the pressure-dependent calculations, they will also indirectly affect the steepness of the PESs from the saddle-point inward. Furthermore, errors in the adduct energetics are indicative of likely errors in the transition state properties. The HF results appear to severely underestimate the binding energy of all four adducts. The B3LYP/6-31G** results overestimate the binding energies of all the adducts and overestimate the relative stability of adducts **1** and **4** as compared to **2** and **3**. The B3LYP/6-311++G** results are in qualitative agreement with the higher level results, though they are not at the accuracy one would require for quantitative kinetics calculations. This large improvement over the B3LYP/6-31G** results reflects a strong dependence on basis set. The MP2 and MP4 results determine all four well depths to be within 10 kcal/mol of one another.[29] This is inconsistent with all other calculations performed. The roMP2 results restrict the paired electrons and include diffuse functions in the basis sets, improving upon the MP2 energies. The PMP4 results for the relative well depths are most closely aligned with those employed in the present study. The present computational scheme was applied to the ethylene−OH system, where the PES has already been used to very accurately determine rate constants varying both temperature and pressure, and the present computational scheme reproduces the ethylene−OH well depth to within 0.8 kcal/mol. The pressure dependence for the ethylene−OH system is particularly sensitive to the well-depth.

An illustrative plot of the potential energy surfaces for formation of the four isomers (**1**−**4**) in the region of the inner transition state is shown in Figure 2. The energies seen in Figure 2 do not include zero point energy. Isomers **1** and **4** (corresponding to the more stable, allylic radicals) have significantly larger binding energies, and thusly steeper PESs in the region between the inner saddle points and the deep wells of the adducts. The most notable feature of these PESs is that the inner saddle points to formation of each of the four isoprene−OH adducts are found *below* the reaction asymptote. This result is contrary to those previously reported by Francisco-Marquez et al.,[39] which suggested that formation of isomers **2** and **3** involves surmounting a barrier above the OH−isoprene reaction asymptote (Table 4). In such a model, the rates of formation of isomers **1** and **4** are so much faster than for isomers **2** and **3** that isomers **2** and **3** should never be formed at room temperature. Experimental studies support the formation of isomers **2** and **3** in non-negligible quantities.[31]

TABLE 4: Energies of Stationary Points (kcal/mol) Relative to the Isoprene−OH Asymptote, Including Zero Point Energy

species	energy (kcal/mol)[a]	energy (kcal/mol)[b]
isoprene + OH	0	0
TS 1	−2.4	−1.7
TS 2	−0.9	5.3
TS 3	−0.1	2.7
TS 4	−2.1	−1.8
adduct 1	−37.3	−35.9
adduct 2	−24.9	−20.9
adduct 3	−24.1	−21.0
adduct 4	−35.0	−33.4

[a] Current methodology (eq 1) including zero point energy and the spin orbit splitting of the hydroxyl radical. [b] BHandHLYP/6-311G** level of theory, including zero point energy, as reported by Francisco-Marquez et al.[39]

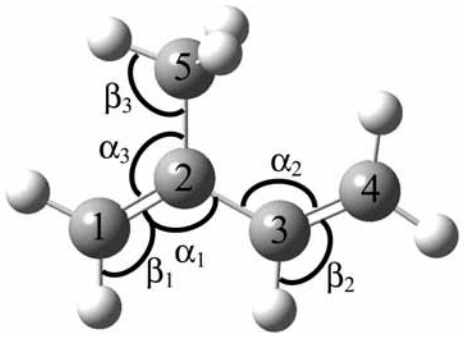

Parameter	B3LYP/6-311++G**	Experiment
C=C	1.342 Å	1.350 Å
C_2-C_3	1.467 Å	1.463 Å
C_2-C_5	1.508 Å	1.512 Å
C_{sp^2}-H	1.084 Å	1.076 Å
C_{sp^3}-H	1.091 Å	1.110 Å
$\angle\alpha_1$	119.7°	121.4°
$\angle\alpha_2$	126.1°	127.3°
$\angle\alpha_3$	121.5°	121.0°
$\angle\beta_1$	121.4°	124.3°
$\angle\beta_2$	118.6°	123.4°
$\angle\beta_3$	111.0°	109.1°

Figure 3. Computationally determined structure of isoprene with relevant geometrical parameters compared to geometrical parameters determined by the gas-phase electron diffraction method presented in ref 55.

Saddle points for isomers **1** and **4** were located using the computational scheme described in eq 1 at 2.35 Å carbon-oxygen separation and 2.3 Å carbon-oxygen separation, respectively, and geometries are provided as Supporting Information. This method was also applied to the location of saddle points for isomers **2** and **3**, where saddle points were located at 2.15 Å carbon-oxygen separation and 2.1 Å carbon-oxygen separation, respectively. These saddle points are in relatively good agreement with those found on the B3LYP surface at 2.08 Å carbon-oxygen separation and 2.105 Å carbon-oxygen separation for isomers **2** and **3** and these geometries are also provided as Supporting Information.

B3LYP is known to give credible geometric parameters and frequencies for organic molecules.[54] Traaeteberg et al.[55] experimentally determined structural parameters for isoprene using a gas-phase electron diffraction technique. Experimentally determined geometrical parameters compared with the calculated parameters are in good agreement as seen in Figure 3. In addition, the vibrational frequencies for isoprene are in good agreement with those determined experimentally[55] (Table 1).

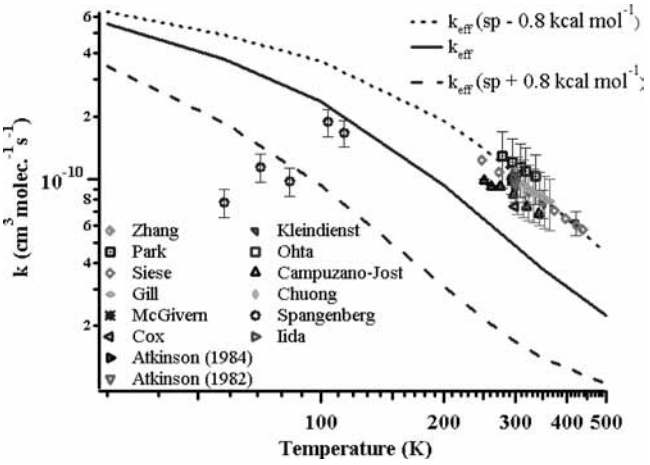

Figure 4. Effective high-pressure rate constants employing a −0.8 kcal mol^{-1} adjustment (dotted line), no adjustment (solid line), and a +0.8 kcal mol^{-1} adjustment (dashed line) to the saddle point energy as a function of temperature for all four isoprene−OH adducts compared to experimental data (Zhang,[30] Kleindienst,[23] Park,[26] Ohta,[25] Siese,[27] Campuzano-Jost,[18] Gill,[21] Chuong,[20] McGivern,[24] Spangenberg,[28] Cox,[19] Iida,[22] Atkinson,[14] Atkinson[15]).

High-frequency motions are reasonably described by harmonic oscillator potentials and errors in these frequencies do not result in large errors in the rate predictions. Moreover, as rate calculations involve ratios of partition functions, one can often expect cancellation of errors. First, the frequency calculations for both species need to be performed at the same level of theory. Second, the conserved modes would be estimated either high or low in the same direction for both the transition state and the reactant(s). It is clear that only the lowest frequency motions, on the order of a couple hundred cm^{-1} need to be considered as a possible source of error to the kinetics evaluations. We treat the majority of these low-frequency motions as hindered rotors,[56] which should provide a sufficiently accurate treatment.

B. Rate Calculations. *Rate Constants in High-Pressure Limit.* In calculating the capture rate on the long-range part of the potential for OH addition to isoprene, it is not obvious, a priori, which electrostatic interaction will be dominant. Capture rates considering the dipole−quadrupole, dipole−dipole, dipole−induced dipole, and dispersion forces were all considered as well as a capture rate considering the sum of these interactions (where the sum is dominated by dispersion forces). The temperature-dependent capture rates for the various interactions can be found in Table 2.

The present predictions for the OH + isoprene rate constant in the high-pressure limit are illustrated in Figure 4, together with the available experimental data. The solid line in Figure 4 is the simulation excluding any adjustment to the ab initio determined saddle point energy. A modest adjustment in the saddle point energy to formation of each OH−isoprene adduct of −0.8 kcal/mol yields high-pressure rate constants in better agreement with the experimentally determined rate constants, as can be seen by the higher dotted line in Figure 4. The adjustment affords a 300 K rate constant of 1.06×10^{-10} cm^3 molecule^{-1} s^{-1}, which is in good agreement with the recommended value. The lower dashed line reflects an increase in the saddle point energy of 0.8 kcal/mol. Nearly all of the available high-pressure limit rate constants fall within a few percent of the dotted line. A consistent use of the saddle point adjustment of −0.8 kcal/mol was chosen on the basis of the excellent agreement between the model and the high-pressure limit data.

This decrease is similar to what was found to be necessary for describing the reaction kinetics in the OH−ethylene system. Importantly, this decrease in the ab initio predicted saddle point is well within the expected uncertainty of the quantum chemical calculations and should be considered as a likely error in these calculations. Errors of this magnitude are consistent with multireference effects of the wavefunction using the employed ab initio methodology. Benchmarking with the ethylene−OH case, however, offers substantial confidence to the accuracy of this methodology and as an analogous model, one expects a decrease on the order of ∼1 kcal/mol to the predicted saddle point energy.

The lower rate constants, when compared to the average in Figure 4, by Campuzano-Jost et al.,[18] are in very good agreement with the temperature dependence seen. In that work, isoprene concentrations were measured in situ via UV absorption. The authors note that an error in the absorption cross section of isoprene would directly translate to a systematic error in the measured rate constants. The faster than average rate constants determined by Park et al.[26] are likely due to the difficulties in accurately extrapolating low-pressure measurements to the high-pressure limit.

The low-temperature data points of Spangenberg et al.[28] are consistent with an appreciable positive temperature dependence of approximately $T^{3/2}$. Such a temperature dependence differs from standard long-range electrostatic capture rates and may be the result of errors due to the challenges associated with low-temperature measurements and the authors cite several sources of plausible error. Similar low-temperature experiments have been employed for the addition of OH to ethylene, propene, and 1-butene[57] and to a series of butenes.[58] In these studies, a monotonic increase in the observed rate constants with a decrease in temperature is observed. An explanation for the substantial differences in the temperature dependence exhibited in the OH addition to isoprene is not obvious. One would expect, as the present calculations predict, that a similar trend in the low-temperature rate constants would be observed. Sims et al. note that the low-temperature rate constants are only limited by the capture rate. We have shown, in the previous study on the OH addition to ethylene, that inclusion of the long-range electrostatic potential provides rate constant estimates in excellent agreement with those experimentally determined at low temperatures. One aspect of this analysis involved the realization that Leone and co-workers measurements for the ethylene−OH system were not in the high-pressure limit. A similar deviation from the high-pressure limit might help explain some of the discrepancies between our predictions and the Spangenberg et al.[28] measurements. However, explicit master equation simulations indicated that the isoprene−OH system is in the high-pressure limit for the experimental conditions of ref 28.

The reproduction of the observed temperature dependence provides a stringent test for theory. The activation energy, defined as $-R\,\mathrm{d}(\ln k)/\mathrm{d}(1/T)$, has been of interest for this and analogous systems due to its negative value under ambient conditions. This is not quantitatively identical to the negative value of the saddle point energy relative to separated products (threshold energy in a transition state theory context), as has been proposed in previous reports.[39] The present calculations are in excellent agreement with experimental observations, which indicate an Arrhenius activation energy of −1 kcal/mol at room temperature. The calculated activation energy is −0.77 kcal/mol. At higher temperatures, the temperature dependence changes sign due in the large part to the change of mechanism to a predominant hydrogen abstraction mechanism.

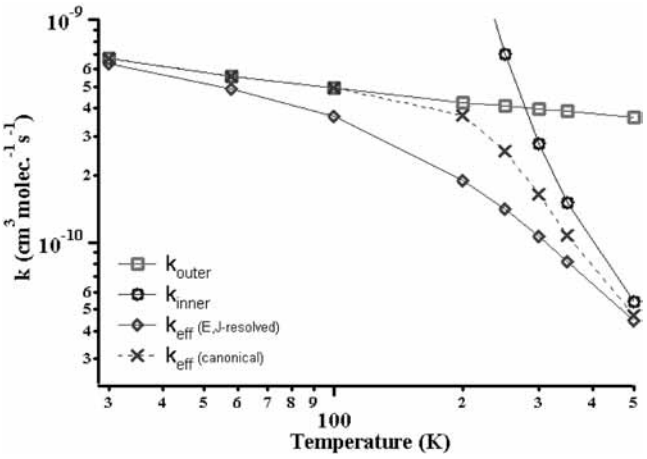

Figure 5. High-pressure rate constants as a function of temperature for the flux through the outer transition state and the inner transition state and for the combined flux through both transition states considering both a combination of flux at the canonical level and a combination of flux at the *E*,*J*-resolved level.

Figure 5 compares the rate coefficients when including only the flux through the outer transition state, only the flux through the inner transition state, and the effective flux when considering both transition states. Furthermore, the dashed line presents the effective rate constants including both the inner and outer transition state rate constants, but combined at the *canonical* level. It is evident that over the entire temperature range, the effects of both transition states are prevalent. At 300 K, there is a 62% reduction in the addition rate upon including the effects of both transition states, at the *E*,*J*-resolved level, as compared to considering the inner transition state alone. Even at 500 K, the rate constant including both transition states is substantially (18%) lower than that determined using only the inner transition state. It is also clear from the results that the flux through each transition state must be combined at the *E*,*J*-resolved level. At 300 K, there is still a 35% reduction in the rate constant achieved by combining flux at the *E*,*J*-resolved level of theory over combining the rate constants at a canonical level. This effect is significant (i.e., by more than 10%) over the entire temperature range from 58 to 350 K.

Although Francisco-Marquez et al.[39] did consider flux through two transition states, the long-range transition state was considered in the context of an equilibrium constant describing the formation and dissociation of a loosely bound van der Waals complex. This treatment relied on the implicit assumption that the van der Waals complexes suffer many collisions before reaction such that a thermal distribution of states is maintained, permitting the use of *canonical* rate constants. The shallowness of the van der Walls wells suggests that this is seldom if ever true in the present reaction. Additionally, their overall rate constant calculation relies on the following expression:

$$k = k_1 k_2/(k_{-1} + k_2) \qquad (6)$$

where a steady-state approximation is assumed. Furthermore, k_{-1} was then assumed to be much larger than k_2, leading to the expression $k = K_{eq}k_2$ over the range of temperatures considered. Such an assumption was invalid in precisely the interesting temperature region where the two transition states provide a comparable bottleneck to the reactive flux.

Branching Ratio Determination. The present predictions for the branching ratios as a function of temperature are provided in Table 5. At room temperature, the branching ratio is determined to be 0.67:0.02:0.02:0.29 (1:2:3:4). This ratio is fairly insensitive to temperature spanning the entire range from 30 to 500 K. Differences in the errors in the quantum chemical estimates for the addition of OH to one of the inner positions of isoprene vs the addition of OH to one of the outer positions may arise from having transition states of different quality (i.e., the transition states to formation of isomers **1** and **4** are looser than those of **2** and **3**). It is reasonable to assume that the errors in the quantum chemical estimates for isomers **1** and **4** (and their corresponding transition states) are of similar magnitude and in the same direction, as is the case for isomers **2** and **3**. However, this is not necessarily the case between the two sets of isomers **1**,**4** and **2**,**3**. To assess the possible impact of errors in the quantum mechanical calculations on the branching ratios, branching ratio ranges are determined.

TABLE 5: Branching Ratios,[a] as a Function of Temperature, for the OH Addition to Isoprene Leading to Formation of Isomers 1−4 at the High-Pressure Limit

	isomers			
temp (K)	**1**	**2**	**3**	**4**
30	0.68 ± 0.03	0.03 ± 0.03	0.01 ± 0.01	0.28 ± 0.01
58	0.68 ± 0.03	0.03 ± 0.03	0.01 ± 0.01	0.28 ± 0.01
100	0.68 ± 0.02	0.03 ± 0.03	0.01 ± 0.01	0.29 ± 0.01
200	0.67 ± 0.02	0.02 ± 0.02	0.01 ± 0.01	0.29 ± 0.01
250	0.67 ± 0.02	0.02 ± 0.02	0.01 ± 0.01	0.29 ± 0.01
300	0.67 ± 0.03	0.02 ± 0.02	0.02 ± 0.01	0.29 ± 0.01
350	0.66 ± 0.03	0.02 ± 0.02	0.02 ± 0.01	0.29 ± 0.01
500	0.64 ± 0.03	0.03 ± 0.02	0.03 ± 0.02	0.30 ± 0.01

[a] Branching ratio range determination is explained in the text.

High-pressure limit rate calculations were performed where the saddle point energies of the dominant pathways (formation of isomers **1** and **4**) were held at constant saddle point reductions of 0.8 kcal/mol for each saddle point and the other two saddle point energies were adjusted by ±1 kcal/mol of this adjustment (i.e., saddle points corresponding to each of isomers **2** and **3** were adjusted up by a total of 0.2 kcal/mol and down by a total of 1.8 kcal/mol). Such adjustments are fairly representative of the possible errors in the relative barrier heights. Although this adjustment has only a minimal effect on the total rate constant, as there is only a few percent contribution from the inner addition positions, the effect on the branching ratio is more substantial. The ± limits on the branching ratios were calculated in this way (Table 5).

We find that the branching ratios are insensitive to changes in pressure, and as shown in Table 5, relatively insensitive to temperature. The branching ratios determined here are in good agreement with those determined previously using structure additivity relationships. Structure additivity relationships yield a branching ratio of 0.618:0.044:0.044:0.294 for isomers **1**−**4**, respectively.[36] Lee et al.[38] adopted the branching ratio proposed by Jenkin[59] of 0.60:0.05:0.05:0.31 (**1**:**2**:**3**:**4**) in the interpretation of their experimental result. The work of Park et al.[26] included a branching of 93% OH addition to the terminal positions of isoprene in the extension of their cycling mechanism used to predict the first generation end product distribution with good agreement with the reports of Atkinson,[60] Jenkin,[59] Zhao,[61] and Paulson.[62]

In the work of Stevens et al.,[29] termolecular rate constants were calculated in the low-pressure limit and a branching ratio of 0.72:<0.01:<0.01:0.28 (**1**:**2**:**3**:**4**) was determined. The authors argued that an equal production of all four isomers under tropospheric conditions was likely because the differences between the transition states would be negligible, leading to adduct formation of comparable yields for all four isomers. In the model presented by McGivern et al.,[24,40] a simple Morse

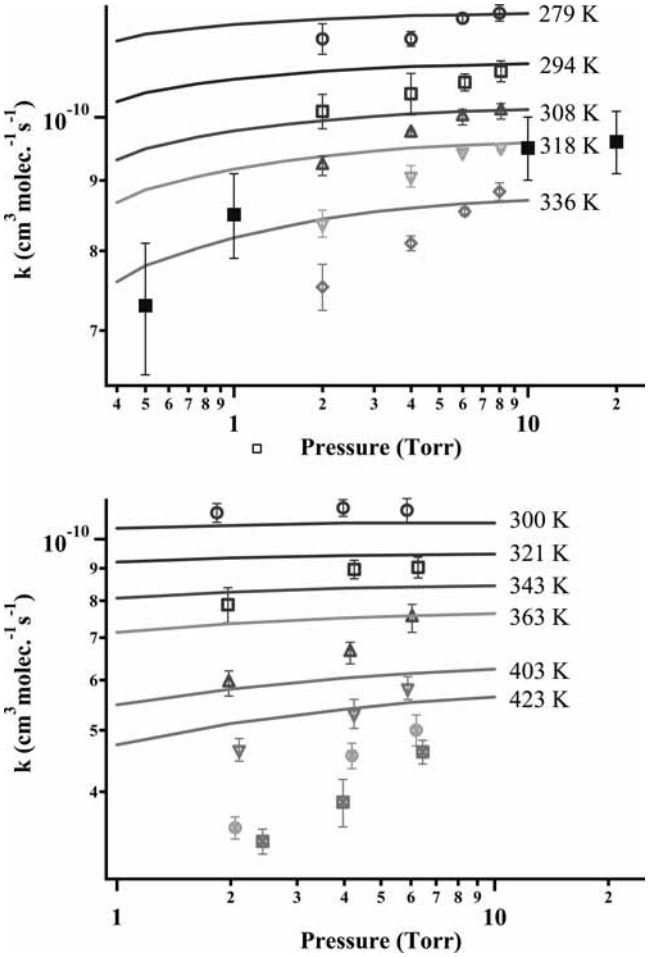

Figure 6. (A) Effective rate constants as a function of pressure (in Ar carrier gas) for all four isoprene−OH adducts compared to the experimental works of Park et al.[26] (open symbols) and the experimental works of McGivern et al.[24] at 295 K (closed symbols). (B) Effective rate constants as a function of pressure (in He carrier gas) for all four isoprene−OH adducts compared to the experimental works of Chuong et al.[31]

function is used to represent the potential energy surface of the OH addition to form each of the four isoprene−OH adducts (**1**−**4**). Rates of reaction were then determined by employing variational RRKM theory. That work presents a computational result of 0.56:0.023:0.046:0.37 (**1**:**2**:**3**:**4**), which is in general agreement with the present result. Their monotonically increasing potential energy surface (PES) neglects reaction coordinate saddle points and other (PES) intricacies. Of particular importance at low to moderate temperatures, these treatments neglect a proper inclusion of the outer transition state. The work of Francisco-Marquez et al.[39] excludes contributions from OH addition to either of the internal positions due to inner transition states that lie above the reaction asymptote. The reported branching ratio is 0.69:0.00:0.00:0.31 (**1**:**2**:**3**:**4**).

It is noteworthy that the absolute energies of the inner saddle points are not the only factors that determine the branching ratio of the OH−isoprene adducts, though this is the most significant factor. Another contribution to each rate is dictated by geometrical parameters. Saddle points are located at carbon−oxygen separations of 2.35, 2.08, 2.105, and 2.3 Å for isomers **1**−**4**, respectively. Saddle points are found at larger carbon−oxygen separations for isomers **1** and **4** and the corresponding motions for these transition states are slightly looser, contributing to faster rates. For example, the imaginary frequencies (denoted with an "i" in Table 1) are, on average, approximately 40% larger for saddle points **2** and **3** as compared to saddle points **1** and **4**. For all of the frequencies below ∼700 cm^{-1}, saddle points **1** and **4** are markedly smaller than the corresponding frequencies in saddle points **2** and **3**.

Pressure-Dependent Rate Constants. We have performed master equation simulations of the pressure dependence in both Ar and He carrier gases. The results for each case employing a downward energy transfer parameter, $\langle \Delta E_{down} \rangle$, of $150(T/298)^{0.7}$ cm^{-1} are illustrated in Figure 6. Included in the figure are experimental observations for Ar (top panel) and He (bottom panel). This functional form for the energy transfer parameter was employed previously in the master equation simulations of the OH addition to ethylene, where the pressure-dependent calculations provided an excellent fit to experimental data. In the ethylene−OH case, the falloff regime spans much higher pressures (up to several hundred Torr) and accurate determination over a large data set in this regime provides a stringent test for the theoretical model.

The isomerization between adduct isomers has not been considered in the present simulations. Lei et al.[40] determined barriers to isomerization at the CCSD(T)/6-311G**//B3LYP/6-31G** level of theory and RRKM/ME calculations were used to assess the impact of the isomerization reactions on the overall pressure dependence of the OH addition to isoprene. Isomerization rates were found to be 3 orders of magnitude slower than dissociation rates and, therefore, considered to have a negligible impact on the overall kinetics. The slow isomerization rates, despite comparable barrier heights to adduct dissociation, are a result of the tightness of the isomerization transition states compared to the loose nature of the transition states associated with adduct formation/dissociation. Additionally, the authors reported that the isomerization pathway had a negligible effect on the branching into the four isoprene-adduct wells.

The results of Park et al. (open symbols)[26] and McGivern et al. (solid symbols)[24] for the pressure dependent rate constants are presented in the upper panel of Figure 6. The data of McGivern et al. were measured at the single temperature of 295 K. As discussed previously, the extrapolation to the infinite pressure limit provided by a Troe Formalism fit in each case, compared to the recommended value at 298 K, indicates that the values reported by McGivern et al. are slightly low, whereas the values of Park et al. are slightly high. We note that a 298 K value of $\langle \Delta E_{down} \rangle = 50$ cm^{-1} provides a much better fit to the available data measured in Ar; however, this is a low value for the energy transfer parameter. Considering the challenges associated with measurements of low-pressure rate constants, we find reasonable agreement between the present calculations and the available pressure-dependent data.

The pressure-dependent results of Chuong and Stevens[31] are presented for a series of temperatures in the lower panel of Figure 6. We are unsure of the origins of the differences between our calculations and the experimental data at higher temperatures. The discrepancy may suggest that the experimental rates have a systematic error, which caused an underestimation in the lower pressure rates at higher temperatures and lead to the strong pressure dependence. Alternatively, some aspect of the pressure-dependent calculations causes an overly gradual approach to the high-pressure limit for these temperatures.[63]

IV. Conclusions

We have extended the previously developed two-transition state model for OH addition to ethylene to the case of OH addition to isoprene. We have calculated the rates of reaction under ambient conditions as well as examined low-temperature

rates of reaction and rates of reaction as a function of pressure and temperature in the falloff regime. We combined phase space theory calculations with standard RRKM theory calculations to determine the contribution to the rates of reaction from both an outer and an inner transition state.

With a modest adjustment of the saddle point energies to each of the four OH−isoprene isomers (**1**−**4**) of −0.8 kcal/mol, we were able to accurately reproduce the high-pressure limit, temperature-dependent rate constants. The high-pressure limiting 300 K rate constant of the OH addition to isoprene calculated here of 1.06×10^{-10} cm^3 molecule^{-1} s^{-1} is consistent with the recommended value. The theoretically predicted capture rate is reproduced to within 10% by the expression $[1.71 \times 10^{-10}(T/298)^{-2.58} \exp(-608.6/RT) + 5.47 \times 10^{-11}(T/298)^{-1.78} \times \exp(-97.3/RT)$; with $R = 1.987$ and T in K] cm^3 molecule^{-1} s^{-1} over the 30−500 K range. A 300 K, a high-pressure limit branching ratio of 0.67:0.02:0.02:0.29 was determined for isomers, **1**−**4**, respectively. An Arrhenius activation energy of −0.77 kcal/mol was determined for the high-pressure addition rate constants around 300 K. The branching ratio was determined to be relatively insensitive to changes in temperature and independent of pressure. Using reasonable parameters for collisional energy transfer in the exponential down model, we were able to satisfactorily reproduce the pressure dependence of these reactions at a variety of temperatures in Ar and He buffer gases.

Acknowledgment. E.E.G. and S.W.N. gratefully acknowledge the support of the National Science Foundation (Grant No. CHE-0204705), the Environmental Protection Agency (Grant No. R03-0132), and the Texas Advanced Research Program (Grant No. 010366-0306). E.E.G. and S.W.N. also acknowledge the Combustion Research Facility at Sandia for visits to the CRF, Dr. Daniel A. Singleton for helpful discussions, Dr. Lisa M. Pérez and the Laboratory for Molecular Simulation and Texas A&M Supercomputing for facilities, software, and support. E.E.G. and S.W.N. also acknowledge Argonne National Laboratories for computing resources and support (Y.G. and S.J.K.). This work is supported by the Division of Chemical Sciences, Geosciences, and Biosciences, the Office of Basic Energy Sciences, and the U.S. Department of Energy. The work at Argonne is supported under DOE Contract Number DE-AC02-06CH11357. Sandia is a multiprogram laboratory operated by Sandia Corporation, a Lockheed Martin Company, for the National Nuclear Security Administration under contract DE-AC04-94-AL85000.

Supporting Information Available: Cartesian coordinates. This material is provided free of charge via the Internet at http://pubs.acs.org.

References and Notes

(1) Finlayson-Pitts, B. J.; Pitts, J. N., Jr. *Chemistry of the Upper and Lower Atmosphere*; Academic Press: San Diego, 2000.

(2) Fuentes, J. D.; Lerdau, M.; Atkinson, R.; Baldocchi, D.; Bottenheim, J. W.; Ciccioli, P.; Lamb, B.; Geron, C.; Gu, L.; Guenther, A.; Sharkey, T. D.; Stockwell, W. *Bull. Am. Meteor. Soc.* **2000**, *81*, 1537.

(3) Guenther, A.; Hewitt, C. N.; Erickson, D.; Fall, R.; Geron, C.; Graedel, T.; Harley, P.; Klinger, L.; Lerdau, M.; et al. *J. Geophys. Res.* **1995**, *100*, 8873.

(4) Kroll, J. H.; Ng, N. L.; Murphy, S. M.; Flagan, R. C.; Seinfeld, J. H. *Geophys. Res. Lett.* **2005**, *32*, L18808.

(5) Kroll, J. H.; Ng, N. L.; Murphy, S. M.; Flagan, R. C.; Seinfeld, J. H. *Environ. Sci. Technol.* **2006**, *40*, 1869.

(6) Surratt, J. D.; Murphy, S. M.; Kroll, J. H.; Ng, N. L.; Hildebrandt, L.; Sorooshian, A.; Szmigielski, R.; Mermeylen, R.; Maenhaut, W.; Claeys, M.; Flagan, R. C.; Seinfeld, J. H. *J. Phys. Chem. A* **2006**, *110*, 9665.

(7) Dommen, J.; Metzger, A.; Duplissy, J.; Kalberer, M.; Alfarra, M. R.; Gascho, A.; Weingartner, E.; Prevot, A. S. H.; Verheggen, B.; Baltensperger, U. *Geophys. Res. Lett.* **2006**, *33*, L13805.

(8) Edney, E. O.; Kleindienst, T. E.; Jaoui, M.; Lewandowski, M.; Offenberg, J. H.; Wang, W.; Claeys, M. *Atmos. Environ.* **2005**, *39*, 5281.

(9) Lim, H.-J.; Carlton, A. G.; Turpin, B. J. *Environ. Sci. Technol.* **2005**, *39*, 4441.

(10) Altieri, K. E.; Carlton, A. G.; Lim, H.-J.; Turpin, B. J.; Seitzinger, S. P. *Environ. Sci. Technol.* **2006**, *40*, 4956.

(11) Carlton, A. G.; Turpin, B. J.; Lim, H.-J.; Altieri, K. E.; Seitzinger, S. *Geophys. Res. Lett.* **2006**, *33*, L06822.

(12) Santos, L. S.; Dalmázio, I.; Eberlin, M. N.; Claeys, M.; Augusti, R. *Rapid Commun. Mass Spectrom.* **2006**, *20*, 2104.

(13) Despite a range of 7.4 x 10^{-11} to 1.1 x 10^{-10} cm^3 molecule^{-1} s^{-1} throughout the literature, a general consensus has been reached that the literature value of the OH addition to isoprene converges to 1.0 x 10^{-10} molecule^3 cm^{-3} s^{-1}.

(14) Atkinson, R.; Aschmann, S. *Int. J. Chem. Kinet.* **1984**, *16*, 1175.

(15) Atkinson, R.; Aschmann, S. M.; Winer, A. M.; Pitts, J. N., Jr. *Int. J. Chem. Kinet.* **1982**, *14*, 507.

(16) Atkinson, R. *J. Phys. Chem. Ref. Data* **1994**, *2*, 1.

(17) Atkinson, R. *Chem. Rev.* **1985**, *85*, 69.

(18) Campuzano-Jost, P.; Williams, M. B.; D'Ottone, L.; Hynes, A. *Geophys. Res. Lett.* **2000**, *27*, 693.

(19) Cox, R. A.; Derwent, R. G.; Williams, M. R. *Environ. Sci. Technol.* **1980**, *14*, 57.

(20) Chuong, B.; Stevens, P. S. *J. Geophys. Res.* **2002**, *107*, 4162.

(21) Gill, K. J.; Hites, R. A. *J. Phys. Chem. A* **2002**, *106*, 2538.

(22) Iida, Y.; Obi, K.; Imamura, T. *Chem. Lett.* **2002**, *8*, 792.

(23) Kleindienst, T. E.; Harris, G. W.; Pitts, J. N., Jr. *Environ. Sci. Technol.* **1982**, *16*, 844.

(24) McGivern, W. S.; Suh, I.; Clinkenbeard, A. D.; Zhang, R.; North, S. W. *J. Phys. Chem. A* **2000**, *104*, 6609.

(25) Ohta, T. *J. Phys. Chem.* **1983**, *87*, 1209.

(26) Park, J.; Jongsma, C. G.; Zhang, R.; North, S. W. *J. Phys. Chem. A* **2004**, *108*, 10688.

(27) Siese, M.; Koch, R. Fittschen, C.; Zetzsch, C. *The Proceedings of EUROTRAC Symposium '94*; Borrell, PmM., et al., Eds.; SPB Academic Publishing bv.: The Hague, The Netherlands, 1994; pp 115−119.

(28) Spangenberg, T.; Köhler, S.; Hansmann, B.; Wachsmuth, U.; Abel, B.; Smith, M. A. *J. Phys. Chem. A* **2004**, *108*, 7527.

(29) Stevens, P. S.; Seymour, E.; Li, Z. *J. Phys. Chem. A* **2000**, *104*, 5989.

(30) Zhang, R.; Suh, I.; Lei, W.; Clinkenbeard, A.; North, S. W. *J. Geophys. Res.* **2000**, *105*, 24627.

(31) Chuong, B.; Stevens, P. S. *J. Phys. Chem. A* **2000**, *104*, 5230.

(32) Atkinson, R.; Arey, J. *Atmos. Environ.* **2003**, *37*, S197.

(33) Park, J.; Jongsma, C. G.; Zhang, R.; North, S. W. *Phys. Chem. Chem. Phys.* **2003**, *5*, 3638.

(34) Greenwald, E. E.; Anderson, K. C.; Park, J.; Kim, K.; Reich, B. J. E.; Miller, S. A.; North, S. W. *J. Phys. Chem. A* **2005**, *109*, 7915.

(35) Greenwald, E. E.; Ghosh, B.; Anderson, K. C.; North, S. W. Manuscript in preparation.

(36) Peeters, J.; Boullart, W.; Hoeymissen, J. V. *The Proceedings of EUROTRAC Symposium '94*; Borrell, PmM., et al., Eds.; SPB Academic Publishing bv: The Hague, The Netherlands, 1994; Vol. 14, p 110.

(37) Peeters, J.; Boullart, W.; Pultau, V.; Vanderberk, S.; Vereecken, L. *J. Phys. Chem. A* **2007**, ASAP.

(38) Lee, W.; Baasandorj, M.; Stevens, P. S.; Hites, R. A. *Environ. Sci. Technol.* **2005**, *39*, 1030.

(39) Francisco-Márquez, M.; Alvarez-Idaboy, J. R.; Galano, A.; Vivier-Bunge, A. *Phys. Chem. Chem. Phys.* **2003**, *5*, 1392.

(40) Lei, W.; Zhang, R. J.; McGivern, W. S.; Derecskei-Kovacs, A.; North, S. W. *Chem. Phys. Lett.* **2000**, *326*, 109.

(41) Greenwald, E. E.; North, S. W.; Georgievskii, Y.; Klippenstein, S. J. *J. Phys. Chem. A* **2005**, *109*, 6031.

(42) Georgievskii, Y. and Klippenstein, S. J. *J. Chem. Phys.* **2005**, *122*, 194103.

(43) Lee, C.; Yang, W.; Parr, R. G. *Phys. Rev. B* **1988**, *37*, 785. Miehlich, B.; Savin, A.; Stoll, H.; Preuss, H. *Chem. Phys. Lett.* **1989**, *157*, 200. Becke, A. D. *J. Chem. Phys.* **1993**, *98*, 5648.

(44) McLean, A. D.; Chandler, G. S. *J. Chem. Phys.* **1980**, *72*, 5639. Krishnan, R.; Binkley, J. S.; Seeger, R.; Pople, J. A. *J. Chem. Phys.* **1980**, *72*, 650.

(45) Clark, T.; Chandrasekhar, J.; Spitznagel, G. W.; Schleyer, P. v. R. *J. Comp. Chem.* **1983**, *4*, 294. Frisch, M. J.; Pople, J. A.; Binkley, J. S. *J. Chem. Phys.* **1984**, *80*, 3265.

(46) Frisch, M. J.; Trucks, G. W.; Schlegel, H. B.; Scuseria, G. E.; Robb, M. A.; Cheeseman, J. R.; Montgomery, J. A., Jr.; Vreven, T.; Kudin, K. N.; Burant, J. C.; Millam, J. M.; Iyengar, S. S.; Tomasi, J.; Barone, V.; Mennucci, B.; Cossi, M.; Scalmani, G.; Rega, N.; Petersson, G. A.; Nakatsuji, H.; Hada, M.; Ehara, M.; Toyota, K.; Fukuda, R.; Hasegawa, J.; Ishida, M.; Nakajima, T.; Honda, Y.; Kitao, O.; Nakai, H.; Klene, M.; Li,

X.; Knox, J. E.; Hratchian, H. P.; Cross, J. B.; Bakken, V.; Adamo, C.; Jaramillo, J.; Gomperts, R.; Stratmann, R. E.; Yazyev, O.; Austin, A. J.; Cammi, R.; Pomelli, C.; Ochterski, J. W.; Ayala, P. Y.; Morokuma, K.; Voth, G. A.; Salvador, P.; Dannenberg, J. J.; Zakrzewski, V. G.; Dapprich, S.; Daniels, A. D.; Strain, M. C.; Farkas, O.; Malick, D. K.; Rabuck, A. D.; Raghavachari, K.; Foresman, J. B.; Ortiz, J. V.; Cui, Q.; Baboul, A. G.; Clifford, S.; Cioslowski, J.; Stefanov, B. B.; Liu, G.; Liashenko, A.; Piskorz, P.; Komaromi, I.; Martin, R. L.; Fox, D. J.; Keith, T.; Al-Laham, M. A.; Peng, C. Y.; Nanayakkara, A.; Challacombe, M.; Gill, P. M. W.; Johnson, B.; Chen, W.; Wong, M. W.; Gonzalez, C.; Pople, J. A. *Gaussian 03*, revision C.02; Gaussian, Inc.: Wallingford, CT, 2004.

(47) Pople, J. A.; Head-Gordon, M.; Raghavachari, K. *J. Chem. Phys.* **1987**, *87*, 5968.

(48) Head-Gordon, M.; Pople, J. A.; Frisch, M. J. *Chem. Phys. Lett.* **1988**, *153*, 503. Frisch, M. J.; Head-Gordon, M.; Pople, J. A. *Chem. Phys. Lett.* **1990**, *166*, 275. Frisch, M. J.; Head-Gordon, M.; Pople, J. A. *Chem. Phys. Lett.* **1990**, *166*, 281. Head-Gordon, M.; Head-Gordon, T. *Chem. Phys. Lett.* **1994**, *220*, 122. Saebo, S.; Almlof, J. *Chem. Phys. Lett.* **1989**, *154*, 83.

(49) MOLPRO is a package of ab initio programs written by H.-J. Werner, P. J. Knowles, R. Lindh, F. R. Manby, M. Schütz, P. Celani, T. Korona, G. Rauhut, R. D. Amos, A. Bernhardsson, A. Berning, D. L. Cooper, M. J. O. Deegan, A. J. Dobbyn, F. Eckert, C. Hampel, G. Hetzer, A. W. Lloyd, S. J. McNicholas, W. Meyer, M. E. Mura, A. Nicklass, P. Palmieri, R. Pitzer, U. Schumann, H. Stoll, A. J. Stone, R. Tarroni, and T. Thorsteinsson.

(50) Ditchfield, R.; Hehre, W. J.; Pople, J. A. *J. Chem. Phys.* **1971**, *54*, 724. Hehre, W. J.; Ditchfield, R.; Pople, J. A. *J. Chem. Phys.* **1972**, *56*, 2257. Hariharan, P. C.; Pople, J. A. *Mol. Phys.* **1974**, *27*, 209. Gordon, M. S. *Chem. Phys. Lett.* **1980**, *76*, 163. Hariharan, P. C.; Pople, J. A. *Theo. Chim. Acta* **1973**, *28*, 213. Blaudeau, J.-P.; McGrath, M. P.; Curtiss, L. A.; Radom, L. *J. Chem. Phys.* **1997**, *107*, 5016. Francl, M. M.; Pietro, W. J.; Hehre, W. J.; Binkley, J. S.; DeFrees, D. J.; Pople, J. A.; Gordon, M. S. *J. Chem. Phys.* **1982**, *77*, 3654. Binning, R. C., Jr.; Curtiss, L. A. *J. Comp. Chem.* **1990**, *11*, 1206. Rassolov, V. A.; Pople, J. A.; Ratner, M. A.; Windus, T. L. *J. Chem. Phys.* **1998**, *109*, 1223. Rassolov, V. A.; Ratner, M. A.; Pople, J. A.; Redfern, P. C.; Curtiss, L. A. *J. Comput. Chem.* **2001**, *22*, 976.

(51) VARIFLEX, A Program for Flexible Transition State Theory, S. J. Klippenstein, A. F. Wagner, S. H. Robertson, R. C. Dunbar, D. M. Wardlaw, at http://chemistry.anl.gov/chem.dyn/VariFlex/index.html (1999).

(52) Hirschfelder, J. O.; Wigner, E. *J. Chem. Phys.* **1939**, *7*, 616. Miller, W. H. *J. Chem. Phys.* **1976**, *65*, 2216. Chesnavich, W. J.; Bass, L.; Su, T.; Bowers, M. T. *J. Chem. Phys.* **1981**, *74*, 2228. Rai, S. N.; Truhlar, D. G. *J. Chem. Phys.* **1983**, *79*, 6046.

(53) Klippenstein, S. J.; Khundkar, L. R.; Zewail, A. H.; Marcus, R. A. *J. Chem. Phys.* **1988**, *89*, 4761.

(54) Young, D. *Computational Chemistry: A Practical Guide for Applying Techniques to Real World Problems*; Wiley-Interscience: New York, 2001.

(55) Traetteberg, M.; Paulen, G.; Cyvin, S. J.; Panchenko, Y. N.; Mochalov, V. I. *J. Mol. Struct.* **1984**, *116*, 141. (and citations therein including: Compton, D. A. C. *J. Chem. Soc., Perkin Trans. 2* **1977**, 1311).

(56) The contributions from the hindered rotors are obtained from a classical phase space integral based treatment coupled with a Pitzer−Gwinn approximation[56a] to approximately correct for quantum effects, as described in ref 56b. (a) Pitzer, K. S.; Gwinn, W. D. *J. Chem. Phys.* **1942**, *10*, 428. (b) Miller, J. A.; Klippenstein, S. J.; Robertson, S. H. *J. Phys. Chem. A* **2000**, *104*, 7525.

(57) Vakhtin, A. B.; Murphy, J. E.; Leone, S. R. *J. Phys. Chem. A* **2003**, *107*, 10055.

(58) Sims, I. R.; Smith, I. W. M.; Bocherel, P.; Defrance, A.; Travers, D.; Rowe, B. R. *J. Chem. Soc. Faraday Trans.* **1994**, *90*, 1473.

(59) Jenkin, M. E.; Boyd, A. A.; Lesclaux, R. *J. Atmos. Chem.* **1998**, *29*, 267. Jenkin, M. E.; Hayman, G. D. *J. Chem. Soc. Faraday Trans.* **1995**, *91*, 1911.

(60) Atkinson, R.; Aschmann, S. M.; Tuazon, E. C.; Arey, J.; Zielinksa, B. *Int. J. Chem. Kinet.* **1989**, *21*, 593.

(61) Zhao, J.; Zhang, R.; Fortner, E. C.; North, S. W. *J. Am. Chem. Soc.* **2004**, *126*, 2686.

(62) Paulson, S. E.; Flagan, R. C.; Seinfeld, J. H. *Int. J. Chem. Kinet.* **1992**, *24*, 79.

(63) One inadequacy of the present master equation treatment is that it ignores any flux that goes from a well to the van der Waals region and then back to a different well. However, such effects are expected to be minimal and furthermore should increase the stabilization rate and thus make our predictions even more discordant with experiment.

(64) http://srdata.nist.gov (citing Huber, K. P.; Herzberg, G. *Molecular Spectra and Molecular Structure. IV. Constants of Diatomic Molecules*; Van Nostrand Reinhold Co.: New York, 1979).